An Experimental Study on the Flow Visualization in Rapidly Mixed Tubular Flame Burners of Various Swirl Numbers

Baolu Shi [1,*], Jie Hu[2], Ningfei Wang[1], Satoru Ishizuka[2]

[1]School of Aerospace, Beijing Institute of Technology, Beijing, China
[2]Faculty of Engineering, Hiroshima University, HigashiHiroshima, Japan
*corresponding author: shibaolu@bit.edu.cn

Abstract As a new element of flame, tubular flame especially the swirl type has excellent flame characteristics such as negligible heat loss, aerodynamic stability and thermodynamic stability. The premixed swirl type tubular flame has been extensively studied through a variety of burners, and various applications have been proposed and demonstrated for determining the flammability limits, stabilizing a flame in a high speed flow, and obtaining a uniform and large-area laminar flame to heat iron slab or to reduce steel sheet surface. To avoid potential hazards of flame flash back even detonation in premixed mode, an inherently safe technique of rapidly mixed tubular flame combustion has proposed, in which the fuel and the oxidizer are individually and tangentially injected into a cylindrical burner from four rectangular slits. Recently this burner has been successfully adopted to investigate the characteristics of oxygen enhanced combustion of methane, which provides a useful tool to save energy and reduce emissions. The results illustrate that the mixing of fuel and oxidizer plays a vital role in obtaining a stable tubular flame.

To fundamentally investigate the flow field especially the mixing process in the rapidly mixed tubular flame burner, a series of measurements have been made on the flow visualization and velocity distribution with a Particle Image Velocimetry (PIV) system. Two groups of optically accessible quartz burners were designed: in the first group, the width of the rectangular slit was maintained as 2 mm while the length varied from 8 to 64 mm, in which the swirl number (S_w) varied from 2.75 to 0.34; in the second group, the slit width increased from 1 to 3 through 2 mm while maintaining the slit length as 8 mm, in which the swirl number decreased from 5.89 to 1.70 through 2.75. The total flow rate and the mean injection velocity ratio of fuel inlet to oxidizer inlet were also varied to measure the mixing layer thickness through flow visualization in a cross section perpendicular to the tube axis around the center of the burner. Detailed observation shows that the mixing layer thickness around the inlet is dominated by a boundary layer type flow regardless of swirl number and injection velocity ratio. The coefficients for the thickness estimation based on the square root of injection velocity (in reverse relationship) have been summarized. In addition, for a constant total flow rate, the mixing is fastest when the mean injection velocity of each inlet is the same. The flow visualization and the axial velocity distribution in a plane containing the tube axis were also analyzed to illustrate the flow motion downstream of the injection slits. The results demonstrate that a reverse flow appears in the burners of swirl number larger than 0.60.

Keywords: Tubular flame burner, flow visualization, particle image velocimetry (PIV), mixing

1 Introduction

A tubular flame, which is circular in cross section and long in the perpendicular direction, has been investigated experimentally, computationally and theoretically in the past four decades [1, 2]. This type of flame is found to be established in both rotating and non-rotating axisymmetric flow fields, which can be obtained through injecting the fresh gas tangentially and inwardly into a cylindrical combustion tube respectively [1-3]. Due to its special structure, the tubular flame experiences flame stretch and curvature simultaneously, and plenty of fundamental studies [1-6] have been made to investigate the flame structures, flammability limits and the Lewis number effects, etc.

From the viewpoint of practical use, its temperature distribution is symmetric and the hot burned gas is surrounded by the cylindrical flame, therefore heat loss is negligible. In addition, inside the flame is the burned gas of low density whereas outside the flame is the unburned gas of high density, and hence, the flame is aerodynamically stable if the mixture is rotated [3, 6]. Recognizing these merits, various applications have been proposed and demonstrated for determining the flammability limits [3-5], stabilizing a flame in a high speed flow [7], and obtaining a uniform and large-area laminar flame to heat iron slab or to reduce steel sheet surface [8].

For large heat output in practical use, premixed combustion is unsafe because of the occurrence of flame flashback and explosion hazards. Thus, a new technique of rapidly mixed type tubular flame combustion has been proposed [9], in which the fuel and the oxidizer are separately, tangentially injected into a burner. If the fuel and oxidizer are rapidly mixed in a strong centrifugal force field in a tube, after ignition combustion with a laminar, tubular-shaped flame can be established. Since there is no supply line of combustible pre-mixture, flame flashback will never occur.

A great amount of investigations have been made on the rapidly mixed type tubular flame combustion using air or diluted air as the oxidizer. To improve combustion efficiency, hence a reduction of fuel consumption and exhaust emissions, pure oxygen and oxygen enriched combustion has been attempted with the rapidly mixed type tubular flame burners [10-12]. It is found that the stable tubular flame could only be established at lean conditions under the very high oxygen mole fractions, and fuel/oxidizer mixing plays a considerable important role in the establishment of a tubular flame [10, 11].

On the other hand, it is also well known that the mixing of fuel and oxidizer has a great influence on the overall performance of combustion in various kinds of combustors, say, the air breathing engine [13, 14], fluidized bed combustor [15, 16] and jet burner [17-19]. Extensive research has been made on the mixing of fuel and oxidizer in shear or mixing layers formed between two reactant streams in the planar, the curved and the rotating flow conditions. Particularly, swirl is widely utilized to enhance fuel/air mixing, prolong residence time and generate the recirculation zone for flame stabilization, which forms an integral part of many combustion and propulsion systems. Chen and Driscoll [20] have investigated the role of the recirculation vortex in improving fuel/air mixing within swirling flames, in which the effect of swirl on flame length was investigated in detail. The effects of fuel/air mixing on flame structures and NO_x emissions in a swirling flame have been analyzed in swirl burners [21] and jet flames [22]. Most of these studies are based on the turbulent mixing in the swirling flow, while in the current study the mixing in the stretched, swirling and laminar flow field is addressed.

The swirl number, which is the ratio of axial flux of angular momentum to the axial flux of linear momentum [23], in this study is defined based on the input and exit parameters assuming an isothermal flow and a uniform exit axial velocity profile, as given by Eq. (1) in the next section. This parameter plays an important role in determining the occurrence of a reverse flow. Though it is general accepted that when the swirl number exceeds 0.6 a reverse flow is induced [24], a number of swirl numbers exist and not all acquire the critical value of 0.6. For instance, Toh et al. [25] experimentally obtained a higher critical value of 0.94 in the axial plus tangential swirling jet, while Al-Abdeli and Masri [26, 27] addressed the significance of other flow parameters such as the axial velocity or its Reynolds number on the formation of downstream recirculation zone. In the present study, by varying both the inlet length and inlet width, the swirl number increases from 0.34 to 5.89, and the reverse flow phenomenon will be discussed.

To discuss the influences of fuel/oxidizer mixing on the flame characteristics in the strong swirl tubular flame burners, flow visualizations in a cross section perpendicular to the tube axis have been discussed to yield the mixing time and the Damköhler number[10-12]. To obtain a general relation in terms of the mixing layer thickness estimation around the exit of the injection slit, and a full understanding of the mixing downstream of the slit, in the present study, 1) burners with constant inlet width and those with constant length are investigated respectively; 2) from weak to strong swirl intensities are used; 3) both the flow visualizations in a cross section perpendicular to the tube axis and those in a plane containing the tube axis have been discussed in detail.

2 Experimental method

Schematic drawings of the quartz made tubular flame burners used in this study are shown in Fig. 1. There are four rectangular tangential slits (left picture), whose width and lengths are denoted as W and L, respectively. The burners are open on two sides with inner diameter of 16 mm and total length (L^*) of 160 and 120 mm (for L= 8 mm).

To clarify the effects of swirl number on the flow structure and mixing, two groups of burner were made. Table 1 lists the detailed parameters of the configuration. In the first group, the slit width W was maintained as 2 mm, while the length of the injection slit L is decreased from 64 to 8 mm, which gives the swirl number

raising from 0.34 to 2.75; in the second group, L was maintained as 8 mm, while W is decreased from 3 to 1 mm, which increases the swirl number from 1.70 to 5.89. Here the swirl number is defined based on geometry, given by the following equation,

$$S_{\mathrm{w}} = \frac{\pi D_{\mathrm{e}} D_0}{4A_T} \qquad (1)$$

in which D_{e} is the exit throat diameter, D_0 is the diameter of a swirl burner, and A_{T} is the tangential slit area [23]. In this study, D_0 is the combustion tube diameter, D_{e} is approximately determined by subtracting the slit width from the burner diameter, i.e., $D_{\mathrm{e}} = D_0 - W$, and A_{T} is the total cross-sectional area of the injection slits. The resultant swirl number varies from 0.34 to 5.89 in this experiment.

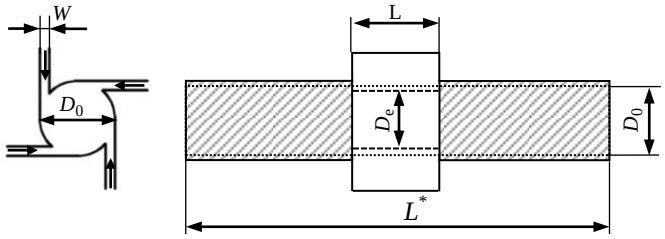

Fig. 1 Schematic of the rapidly mixed type tubular flame burners (quartz made, two-side open).

Table 1
Configuration of the combustor

Cases	Burner diameter D_0 (mm)	Throat diameter D_{e} (mm)	Total length of burner L^* (mm)	Slit width W(mm)	Slit length L(mm)	Swirl number S_{w}
Group1 (W = const.)	16	14	160	2	64	0.34
	16	14	160	2	32	0.69
	16	14	160	2	16	1.37
	16	14	120	2	8	2.75
Group2 (L = const.)	16	13	120	3	8	1.70
	16	14	120	2	8	2.75
	16	15	120	1	8	5.89

To visualize the flow motion, measurements with Particle Image Velocimetry (PIV) were conducted. The setup is shown in Fig. 2. Dry air metered by an orifice flow meter was supplied as the flow gas. Magnesium oxide (MgO) particles with a few microns in diameter were seeded into one stream through a particle seeder, and then the seeded air flow was horizontally injected into two parallel slits, while the non-seeded air flow was injected from the other two. The flow structure and the mixing between the seeded air flow (flow rate of Q_{S}) and the non-seeded air flow (Q_{A}) were recorded by a PIV system.

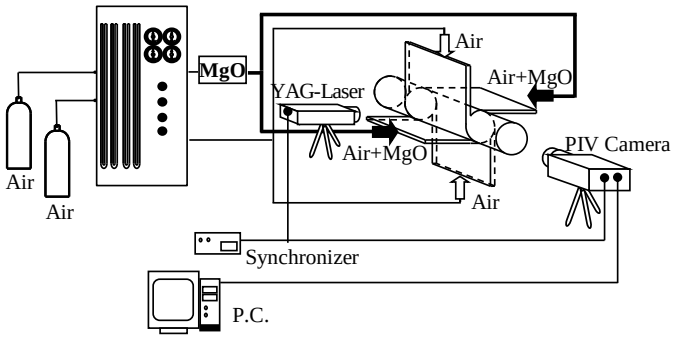

Fig. 2 Schematic of the PIV measurement system.

The PIV system consists of a high-resolution CCD camera (TSI, 1280 × 1024 pixels, 10-bit grayscale), a double-pulsed Nd: YAG laser (120 mJ/pulse, 15 Hz), a host computer, and a synchronizer. The circumferential flow structure around the burner center is measured, in which the double-pulsed laser sheets

were directed to the quartz burner, perpendicularly with respect to the tube axis. As seen in Fig. 2, the camera was mounted to record light scattered along the burner axis through the end of the tube. The laser sheet was positioned near the center of the tube but offset 2 mm from true center for better particle visualization of the mixing layer around the inlets. Since a similar solution exists in the present flow field, the mixing layer thickness remains unchanged at offset positions. When measuring the axial flow field, the laser sheets passed through the tube axis.

3 Results and discussion

3.1 Constant slit width (*W*= 2 mm, Group1)

To examine the flow structure and mixing in the burners of various swirl numbers, with four burners of different slit lengths, the flow in a cross section perpendicular to the tube axis around the burner center and that in a plane containing the tube axis downstream of the slit have been visualized and discussed.

3.1.1 S_w= 0.34

At first, the case with low swirl number of 0.34 is analyzed. Figure 3 shows the flow visualizations in the cross section perpendicular to the tube axis at the injection flow rates of Q_S= Q_A= 0.09 and 0.27 m^3_N/h. Due to the difficulties for visualization, the injection flow rates are very small, which are gradually increased to derive the relation between the measured thickness and the injection velocity (V_t). The Reynolds numbers, defined as V_tW/ν, are 25 and 75. The broken lines show the positions of the tangential slits and the broken circles show the positions of the burner walls. From two horizontal slits of upper left and lower right, dry air seeded with MgO particles was tangentially injected into the burner, while dry air without seeding was injected from two slits of upper right and lower left. A starting point is defined as the inner edge of the lower right slit, which is designated as point *O* in Fig. 3, and a coordinate is taken along the circle. From the starting point, the non-seeded air flow from the upper right slit starts to mix with the seeded air flow from the lower right slit.

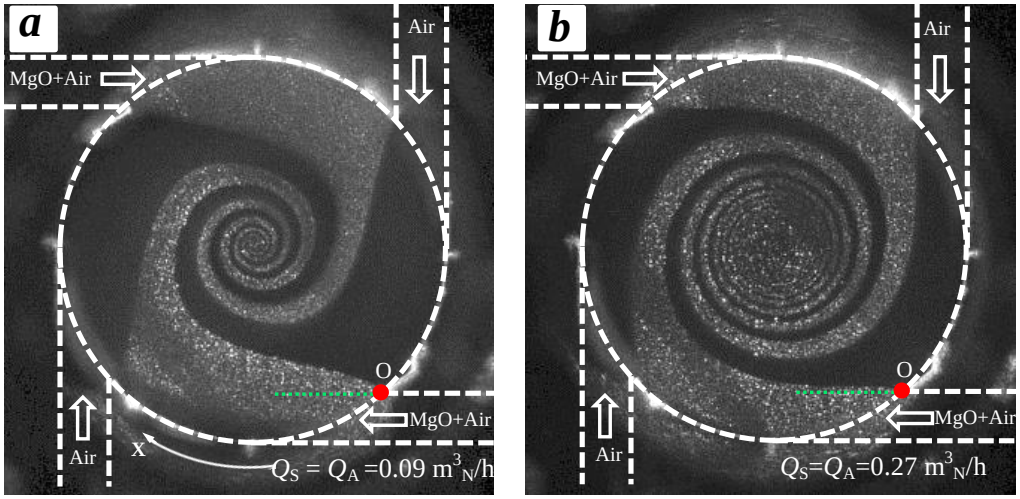

Fig. 3 Flow visualizations in a cross section perpendicular to the tube axis around the center of the burner for various flow rates (Q_S: flow rate of the seeded air flow, Q_A: flow rate of the non-seeded air flow, S_w= 0.34).

In the case of Q_S= Q_A= 0.09 m^3_N/h, as shown in Fig. 3a, the seeded air stream from the lower right slit abruptly expands in width after the flow is ejected from the 2 mm width slit. When the flow goes around its width further expands radially. After meeting the non-seeded air flow from lower left, the seeded flow shrinks in width through an interaction with the air flow from the lower left slit. The air stream from the upper right slit also expands until meets the seeded flow from lower right, thereafter it shrinks in width through the interaction with the flows from the upper left and lower right slits as the stream goes around even approaches the axis of the burner. In the case of Q_S= Q_A= 0.27 m^3_N/h, the widths of the seeded air and air streams are smaller than those of the case 0.09 m^3_N/h, however, they are still slightly larger than the slit width after ejection. The diameter of the well-mixed core increases when the flow rate is further increased to 0.27 m^3_N/h.

The axial flow, which is 10 mm downstream of the slit, has been visualized. The results corresponding to the two conditions in Fig. 3 are shown in Fig. 4. The broken lines show the positions of the inner wall of the quartz tube. When the flow rate is small, $Q_S = Q_A = 0.09$ m^3_N/h, around the center a core with tracer is observed, the diameter of which almost equals to that in the cross section perpendicular to the tube axis (Fig. 3a). When the flow goes further downstream of the slit, the diameter remains almost constant. Outside this core, the air flow layer and the seeded air flow layer alternately appears along the radial direction. Non-seeded zone and seeded zone with large scales are distributed alternately aligned with the axis, which maintain their structures and move parallel along the axis, illustrating that the convection motion normal to the axial direction is weak and the mass diffusion becomes important for mixing.

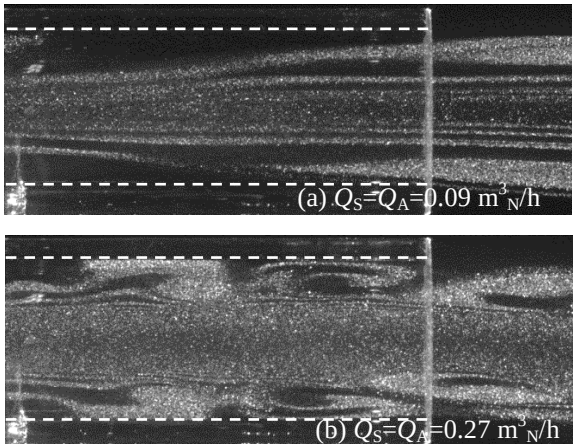

Fig. 4 Flow visualizations along the axis 10 mm downstream of the slit (S_w= 0.34).

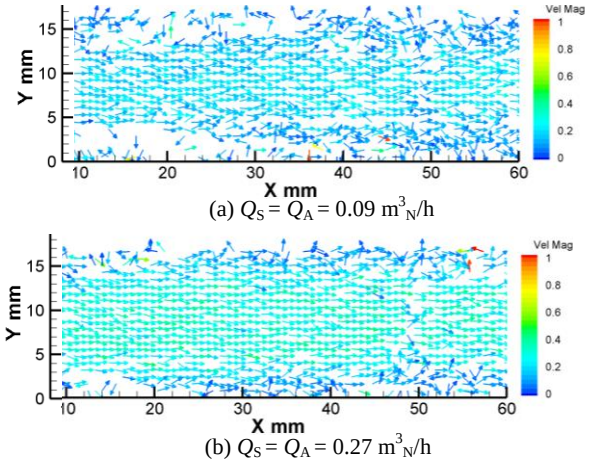

Fig. 5 Axial velocity distributions corresponding to the cases in Fig. 4.

With an increase of the flow rate to $Q_S = Q_A = 0.27$ m^3_N/h, the diameter of the core increases. In addition, almost axisymmetrically distributed periodic flow structures appear around the wall. The length (scale) for the pattern of non-seeded zone which lies between the outer-seeded flow and the inner seeded core, decreases comparing with that of $Q_S = Q_A = 0.09$ m^3_N/h, which illustrates that the mixing between the seeded and non-seeded flows will be completed within a shorter distance, hence a promotion of mixing rate.

It is well known that a recirculation reverse flow may be induced in a swirling flow field. To confirm the motion of the downstream pattern, in Fig. 5, instantaneous vectors corresponding to the flow visualizations in Fig. 4 have been plotted. In the cases of Figs. 5a and 5b, the interval times between the double pulses from the PIV laser were set to 150 and 80 μs. It is seen that the main component of the downstream flow is along the axial direction, and the magnitude around the center is slightly larger. A reverse flow has not been observed.

3.1.2 S_w= 0.69

Next, the case with swirl number of 0.69 is analyzed. Figure 6 shows the flow visualizations in the cross section with the injection flow rates of $Q_S = Q_A = 0.09$, 0.15 and 0.27 m^3_N/h, respectively. In the case of $Q_S = Q_A = 0.09$ m^3_N/h (Fig. 6a), the seeded stream from the lower right slit expands in width after the flow is ejected from the slit. Around the axis, a mixed core is observed. With an increase of the injection flow rate, the width of the flow after ejection decreases. As seen in Fig. 6c, the width of the lower right seeded air flow shrinks after ejected outside the slit, i.e., the width of the seeded flow is smaller than the slit width.

With an increase of the flow rate to 0.15 m^3_N/h, a coaxial cylindrical zone without tracer (as the center broken circle shown) appears in the center. And this diameter increases with an increase of the flow rate. Since the centrifugal force is enhanced with increasing the flow rate, which restrains the high density MgO particles from approaching the axis. On the other hand, since the swirl number becomes larger than 0.6, a reverse flow with tracer particles may be induced, resulting in occasional weak light scattering ine center area.

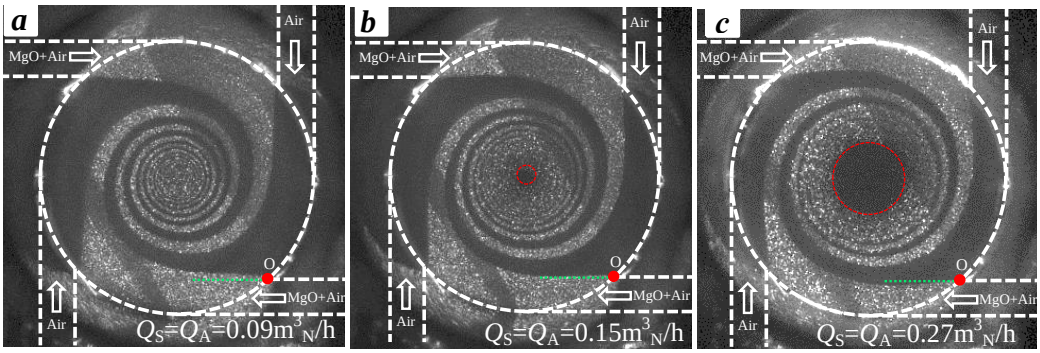

Fig. 6 Flow visualizations in the cross section varying with flow rates (S_w= 0.69).

Figure 7 shows the flow visualizations in the plane containing the tube axis 10 mm downstream of the slit. When the flow rate is small, Q_S= Q_A= 0.09 m^3_N/h (Fig. 7a), the center core is a mixed zone of seeded air and non-seeded air; around the wall large scale non-seeded air zone and seeded air zone distribute alternately along the axis. In the case of Q_S= Q_A= 0.15 m^3_N/h, a series of eye-like patterns appear close to the wall along the axis. A mixed zone is formed further away from the wall, however, the center area is occupied by a flow with few tracers or even without tracer, which corresponds to the non-seeded center zone observed in Fig. 7b. With a further increase of the flow rate to 0.27 m^3_N/h, far downstream of the slit, the seeded air and air are mixed with each other.

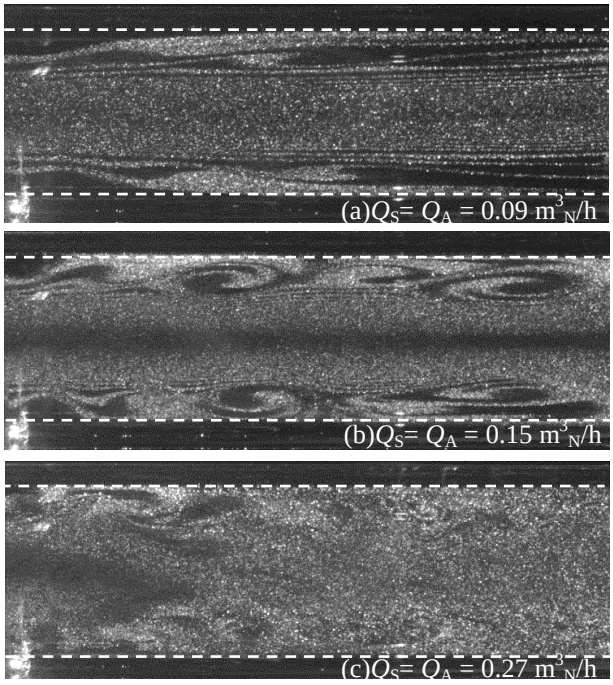

Fig. 7 Flow visualizations in the plane containing the tube axis 10 mm downstream of the slit (S_w= 0.69)

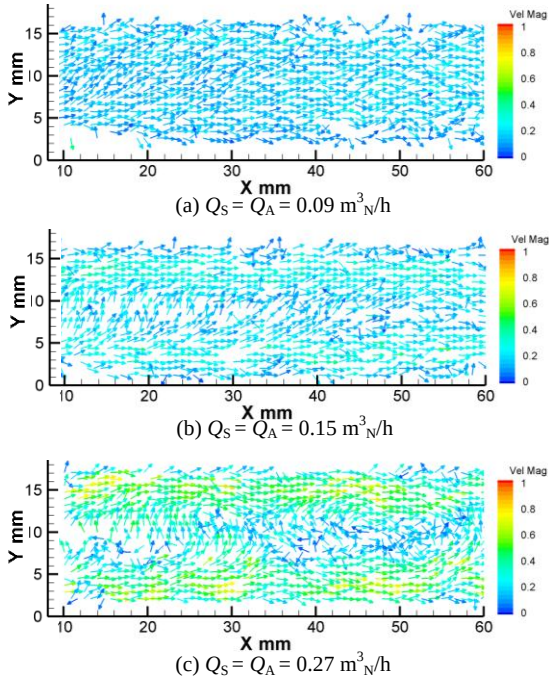

Fig. 8 Axial velocity distributions corresponding to the cases in Fig. 8.

The instantaneous axial velocity distributions for the three cases in Fig. 7 have been examined, and the results are shown in Fig. 8. When the air flow rate is small (Fig. 8a), the main component of the velocity is along the axis; in the case of Fig. 8b, outside the center zone, the flow shows obvious outward motion along the axis; in the center zone, close to the upstream the velocity distribution shows slight recirculation of the flow. In the case of Fig. 8c, around the center vectors oriented in reverse direction are observed, illustrating the existence of the recirculation reverse flow; close to the burner wall, the flow mainly moves out axially with larger magnitude.

3.1.3 S_w= 1.35

Flow visualizations for various flow rates in the burner of L = 16 mm are shown in Fig. 9. At the flow rates of 0.09 m^3_N/h, around the center a non-seeded core with large diameter is observed in the flow visualization. In the case of Q_S= Q_A= 0.21 m^3_N/h, flow instability is observed, which is distributed symmetrically, as the arrows shown in Fig. 9b. Owing to the occurrence of instability, the center area, which would be a reverse flow region with very few tracers as that shown in Fig. 9a, has been occupied by tracers. Downstream of the slit, tracer particles appear in the whole area without being affected by the strong centrifugal force. Thus, the instability plays an important role in determining the flow structure and mixing around the slit and downstream of the slit.

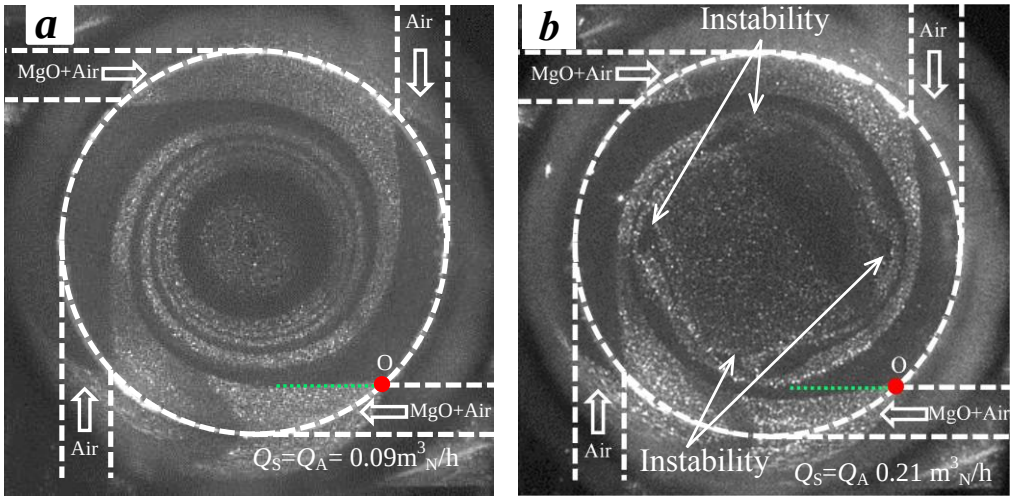

Fig. 9 Flow visualizations around the slit for various flow rates (S_w= 1.37).

3.1.4 S_w= 2.75

The flow visualizations for L = 8 mm have been shown in Fig. 10. In Fig. 10a, it is seen that a core with a recirculation reverse flow appears. However, at a large flow rate, the flow experiences instability around the injection slit, as shown in Fig. 10b. As discussed in section 3.1.3, this instability prompts the mixing downstream of the slit.

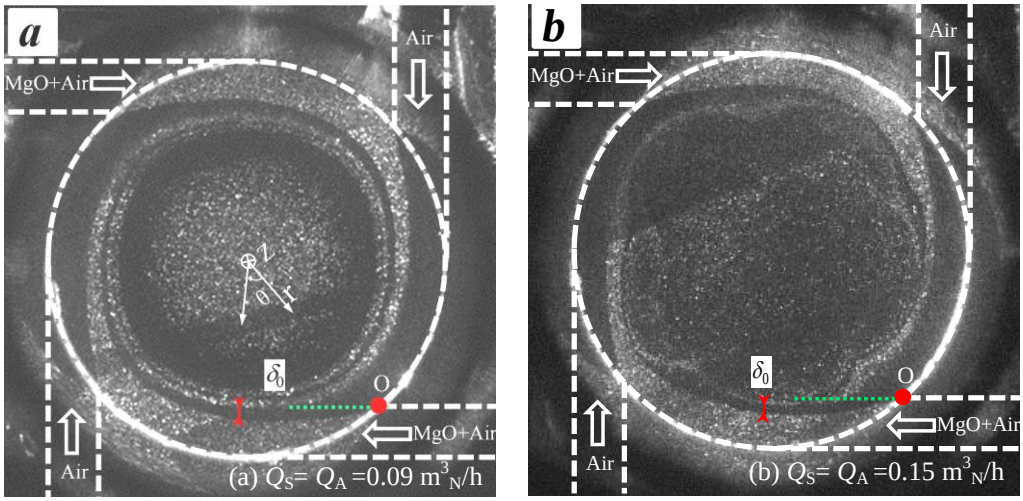

Fig. 10 Flow visualizations around the slit for various flow rates (S_w= 2.75).

3.2 Constant slit length (L= 8 mm, Group 2)

The burners mentioned above adopt constant slit width, while in this section the tubular flame burners with various slit widths but constant slit length are introduced. The slit width reduces from 3 through 2 to 1 mm, giving the swirl number of 1.70, 2.75 and 3.58, respectively. Figure 11 shows the flow visualizations inside

three burners at the injection flow rates of $Q_S = Q_A = 0.069$ m^3_N/h. In the case of $W = 3$ mm, which is shown in Fig. 11a, the seeded flow from the lower right slit abruptly shrinks in width after the flow is ejected from the 3 mm width slit through an interaction with the non-seeded flow from the upper right slit. This non-seeded stream from the upper right slit also shrinks much in width through the interaction with the flow from the upper left, and its width gradually decreases as the stream goes around.

In the case of $W = 2$ mm (Fig. 11b), both widths of the seeded and the non-seeded streams are slightly smaller than those in W=3 mm. As seen in $W = 3$ mm, both flows also shrink in width after the flows are ejected from the 2 mm width slit.

However, in the case of $W = 1$ mm, it is seen in Fig. 11c that the seeded stream from the lower right slit slightly expands in width when the flow is ejected outside from the slit. Thereafter the flow shrinks and the width gradually decreases. The non-seeded air stream from the upper right slit also initially expands and afterward shrinks and its width decreases.

With higher flow rates, the flow patterns as those in Fig. 11 are hard to observed, especially in the case of $W = 1$ mm. However, it is seen that at low flow rates the same flow pattern is observed as those with constant slit width.

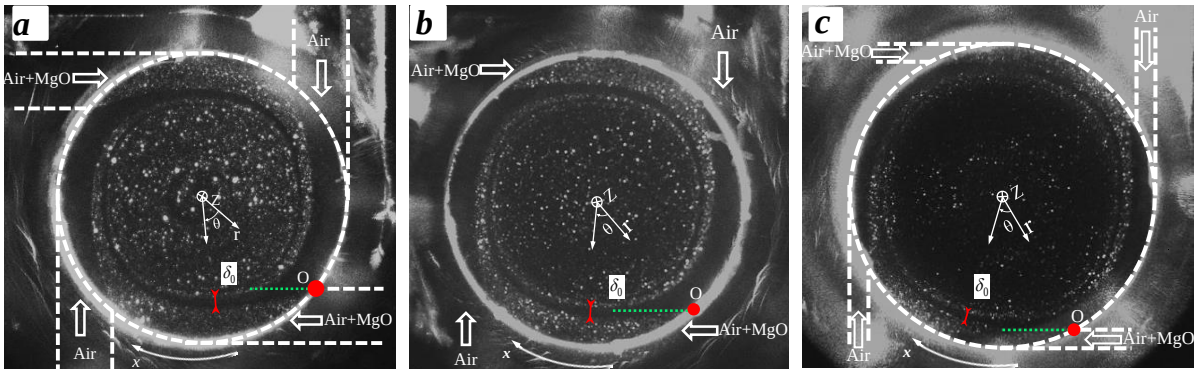

Fig. 11 Flow visualizations in the rapidly mixed type burners ($Q_S = Q_A = 0.069$ m^3_N/h, a: $W = 3$ mm, b: $W = 2$ mm, c: $W = 1$ mm).

3.3 Mixing layer thickness

The mixing between the fuel and the oxidizer plays an important role in determining the tubular flame structure, especially that around the exit of the injection slit. It has been shown that the mixing around the exit of the slit is dominated by a boundary layer type flow [10, 11]. As analyzed in the previous studies[10, 11], from the starting point O, after 45 degree the width of the non-seeded air from the upper right slit has been measured, denoted as δ_0, as shown in Figs. 3, 6, 9,11. It is assumed that for complete mixing, the seeded air flow should diffuse into the non-seeded air stream whose width is δ_0, and consequently δ_0 is assumed as the mixing layer thickness around the exit of the slit. Under various flow rates, in the burners of Group 1 and Group 2, δ_0 values have been examined and the results are plotted in Fig. 12a and 12b, respectively. It is seen that for all the cases the δ_0 is inversely proportional to the square root of the calculated mean injection velocity of the upper right air flow.

As for the coefficients, in the case of $S_w = 0.34$, owing to the expansion of the flow after injection, the value of δ_0 is small hence a small coefficient. Especially, at a very low flow rate (low injection velocity), due to the radial expansion after injection as well as the influences of mass diffusion, the measured δ_0 show some deviation from the inverse square root line. In the cases of $S_w = 0.69$ and 1.37, the coefficients are about 5.0×10^{-4} $[m^{1.5}s^{-0.5}]$, while those for $S_w = 0.34$ and 2.75 are close to 4.03×10^{-4} $[m^{1.5}s^{-0.5}]$, which is the same as that of W= 2 mm in ref. [11], as the broken line shown. The coefficients are the same for $S_w = 0.34$ and 2.75, however, for the same flow rate, the mean injection velocity in the burner of $S_w = 0.34$ is 1/8 that of $S_w = 2.75$, hence a large δ_0, leading to a poor mixing around the exit of the slit.

In Group 2, the coefficients for W= 1 and 3 mm (corresponding swirl number of 5.89 and 1.70) are given as 4.36×10^{-4} $[m^{1.5}s^{-0.5}]$ and 3.51×10^{-4} $[m^{1.5}s^{-0.5}]$, respectively. Based on these measurements, for various swirl numbers, the coefficient varies from 3.51×10^{-4} $[m^{1.5}s^{-0.5}]$ to 5.0×10^{-4} $[m^{1.5}s^{-0.5}]$.

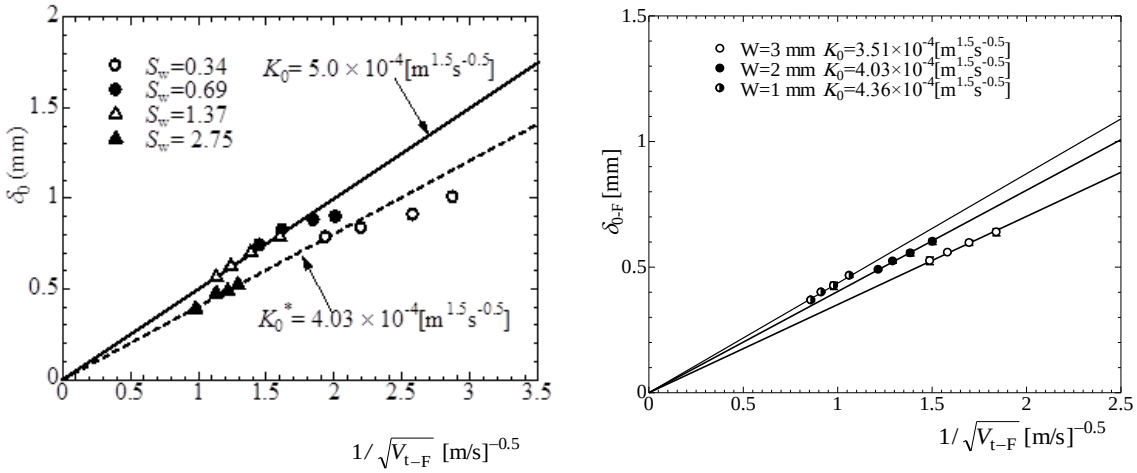

(a) W= const.= 2 mm, Group 1 (b) L= const.= 8 mm, Group 2

Fig. 12 Boundary layer type flow dominating the mixing around the exit of the slit .

3.4 Best mixing condition

In the actual combustion tests, the injection flow rates for the fuel and the oxidizer are usually different. Hence it is very important to investigate the cases with different flow rate ratios of the oxidizer to the fuel. In the low swirl burner of S_w = 0.34, by keeping the total flow rate at about 0.41 m^3_N/h, three cases, with Q_S= 0.5Q_A, Q_S= Q_A and Q_S= 2Q_A, have been investigated. The results are shown in Fig. 13.

Comparing the flow visualizations in the cross section perpendicular to the tube axis (left column), as the non-seeded air flow rate (Q_A) decreases, the width of the air flow from the upper right slit decreases, whereas the lower right seeded air flow gradually expands in width after ejected from the slits. As for the flow downstream of the slit, in the case of Q_S= 0.5Q_A (right of Fig. 13a), close to the non-seeded zone there are highly seeded air zones, which are distributed along the axis outside the center mixed core. In the case of the same injection flow rate (Fig. 13b), highly seeded air zones appear and become larger, whereas the surrounding non-seeded air regions become smaller, illustrating the expansion of mixing zone. When the flow rate of the seeded air is doubled (Fig. 13c), non-seeded air regions are clearly observed. It is seen that the ratio of the flow rates plays an important role in determining the flow structure and mixing downstream of the slit. In specific, with the constant total flow rate, the mixing is best when the injection velocities are equal.

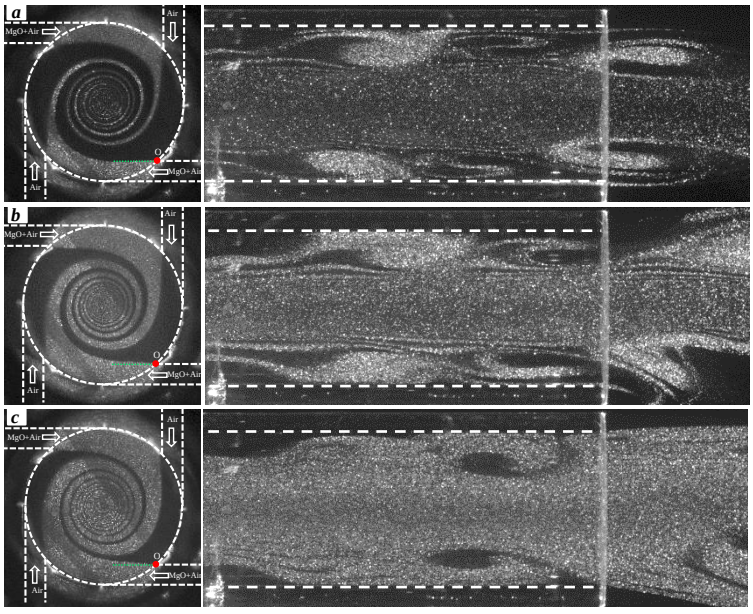

Fig. 13 Flow visualizations for various flow ratios of the seeded air to air at almost constant total flow rate (a: Q_S = 0.135 m^3_N/h, Q_A = 0.27 m^3_N/h; b: Q_S = Q_A = 0.21 m^3_N/h; c: Q_S = 0.27 m^3_N/h, Q_A = 0.135 m^3_N/h, S_w= 0.34).

In addition, using the burner with larger swirl number S_w= 2.75, four cases with the oxidizer flow rates of Q_S =Q_A (two slits), 0.5Q_A, Q_A and 2Q_A are investigated, respectively. The total flow rate was kept at a constant value about 0.103 m^3_N/h. In the first case, as illustratively shown in Fig. 14a, two original seeded slits were blocked. The air stream from upper right shrank slowly until close to the lower left slit, and δ_0 was large, illustrating poor mixing. In the second case, 2Q_S = Q_A = 0.069 m^3_N/h, the non-seeded air stream slightly expanded after ejected outside, while the seeded flow shrank after ejection. In the third case, Q_S = Q_A= 0.051 m^3_N/h, and the same phenomenon as those in Figs. 10a and 11b has been observed. In the last case, which is shown in Fig. 14d, the seeded flow rate was doubled as that of the non-seeded air, Q_S = 2Q_A = 0.069 m^3_N/h. The non-seeded stream abruptly shrank after ejection and shrunk further from the starting point through the interaction with upper left and lower right seeded streams, resulting in a very thin width. Though the non-seeded air stream is thin, the seeded air stream is thick, resulting in also poor mixing.

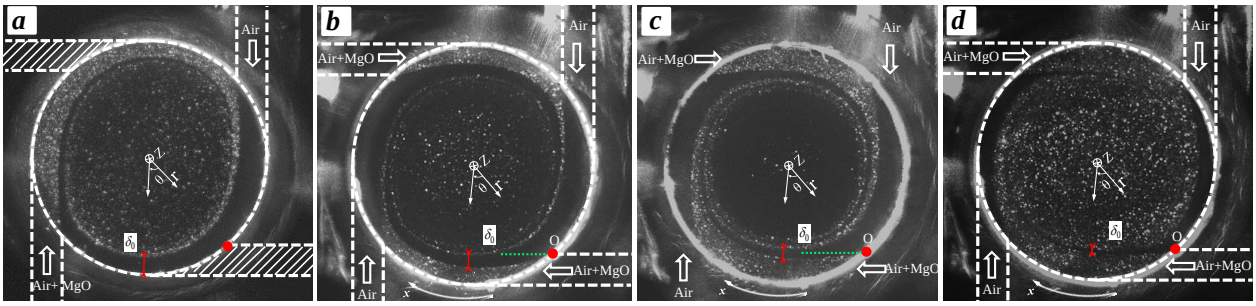

Fig. 14 Flow visualizations for various ratios of the oxidizer to fuel flow rate keeping the total flow rate constant (Q_{Total} = 0.103 m^3_N/h, a: two slits Q_S = Q_A, b: Q_S = 0.5 Q_A, c: Q_S = Q_A, d: Q_S = 2Q_A, S_w= 2.75).

Based on the results of various ratios of seeded flow rate to that of non-seeded flow in both low and large swirl numbers, when the injection velocities from the oxidizer (seeded) and fuel (non-seeded) slits are equivalent, the mixing is best.

4 Conclusions

In this study, flow visualizations in tubular flame burners with various swirl numbers are investigated. The following are specific conclusions:

(1) In the low swirl burner of S_w= 0.34, a reverse flow is not observed, while in the burners of S_w equals to and above 0.69, a reverse flow is observed even at low injection velocity around 1 m/s.
(2) The mixing around the injection slit is dominated by a boundary layer type flow, i.e., the mixing layer thickness is inversely proportional to the square root of mean injection velocity.
(3) At relatively large flow rates, flow instability occurs, which prompts the mixing. However, around the slit exit, the mixing layer thickness maintains its relation with the injection velocity.
(4) Mixing is best when the injection velocities from the oxidizer and fuel slits are equivalent.

References

[1] Ishizuka S, Dunn-Rankin D, Pitz R W, Kee R J, Zhang Y, Takeno T, Shimokuri D (2013) Tubular combustion. Momentum Press, New York.

[2] Wang P, Wehrmeyer J A, Pitz R W (2006) Stretch rate of tubular premixed flames. Combust. Flame 145, pp.401-414.

[3] Ishizuka S (1984) On the behavior of premixed flames in a rotating flow field: establishment of tubular flames, Twentieth Symposium (international) on Combustion/The Combustion Institute, pp.287-294.

[4] Ishizuka S (1991) Determination of flammability limits using a tubular flame geometry. J. Loss Prev. Process Ind. 4, pp.185-193.

[5] Ishizuka S (1989) An experimental study on extinction and stability of tubular flames. Combust. Flame 75, pp. 367-379.

[6] Ishizuka S (1993) Characteristics of tubular flames. Prog. Energy Combust. Sci. 19, pp.187-226.

[7] Shimokuri D, Ishizuka S (2005) Flame stabilization with a tubular flame. Proc. Combust. Inst. 30, pp.399-406.

[8] Ishizuka S, Shimokuri D, Ishii K, Okada K, Takashi K, Suzukawa Y (2009). Development of practical combustion using tubular flames. J. Combust. Soc. Japan. 156, pp.104-113, in Japanese.

[9] Ishizuka S, Motodamari T, Shimokuri D (2007) Rapidly mixed combustion in a tubular flame burner. Proc. Combust. Inst. 31, pp.1085-1092.

[10] Shi B, Shimokuri D, Ishizuka S (2013) Methane/oxygen combustion in a rapidly mixed type tubular flame burner. Proc. Combust. Inst. 34, pp.3369-3377.

[11] Shi B, Shimokuri D, Ishizuka S (2014) Reexamination on methane/oxygen combustion in a rapidly mixed type tubular flame burner. Combust. Flame 161, pp.1310-1325.

[12] Shi B, Hu J, Ishizuka S (2015) Carbon dioxide diluted methane/oxygen combustion in a rapidly mixed type tubular flame burner. Combust. Flame 162, pp.420-430.

[13] Henry J R (1969) Recent research on fuel injection and mixing and piloted-ignition for scramjet combustors. Twelfth Symposium (International) on Combustion/The Combustion Institute pp.1175-1182.

[14] Schetz J A, Gilreath H E, Lubard S C (1969) Fuel injection and mixing in a supersonic stream. Twelfth Symposium (International) on Combustion/The Combustion Institute,pp. 1141-1149.

[15] Ryu C, Shin D, Choi S (2001) Effect of fuel layer mixing in waste bed combustion. Adv. Environ. Res. 5, pp.259-267.

[16] Pallarès D and Johnsson F (2008) Modeling of fuel mixing in fluidized bed combustors. Chem. Eng. Sci. 63, pp.5663-5671.

[17] Hawthorne W R, Weddell D S, Hottel H C (1949) Mixing and combustion in turbulent gas jets. Third symposium on combustion, flame and explosion phenomena , pp.266-288.

[18] Harris R J, Horne W, Williams A (1976) High intensity oxy-methane combustion in a jet-mixing burner. Combust. Flame 26, pp.311-321.

[19] Yin Z, Zhang H, Lin J (2007) Experimental study on the flow field characteristics in the mixing region of twin jets. Journal of Hydrodynamics, Ser. B, Vol. 19, No. 3, pp.309-313.

[20] Chen R H, Driscoll J F (1988) The role of the recirculation vortex in improving fuel-air mixing within swirling flames.Twenty-second Symposium (International) on Combustion/The Combustion Institute, pp.531-540.

[21] Terasaki T, Hayashi S (1996) The effects of fuel-air mixing on NOx formation in non-premixed swirl burners. Twenty-sixth Symposium (International) on Combustion/ The Combustion Institute, pp.2733-2739.

[22] Cheng T S, Chao Y C, Wu D C, Yuan T, Lu C C, Cheng C K and Chang J M (1998) Effects of fuel-air mixing on flame structures and NOx emissions in swirling methane jet flames. Twenty-seventh Symposium (International) on Combustion/The Combustion Institute, pp.1229-1237.

[23] Syred N and Beer J M (1974) Combustion in swirling flows: a review, Combust. Flame 23, pp.143-201.

[24] Beer J M, Chigier N A (1972) Combustion aerodynamics. Applied Science Publishers, London.

[25] Toh I K, Honnery D, Soria J (2010) Axial plus tangential entry swirling jet. Exp Fluids 48, pp.309-325.

[26] Al-Abdeli Y, Masri A R (2003) Recirculation and flow field regimes of unconfined non-reacting swirling flows. Exp. Therm. Fluid Sci. 27, pp.655-665.

[27] Al-Abdeli Y, Masri A R (2004) Precession and recirculation in turbulent swirling isothermal jets. Combust. Sci. Tech. 176, pp.645-665.